Climate Change Projections for the Twenty-First Century and Climate Change Commitment in the CCSM3

GERALD A. MEEHL AND WARREN M. WASHINGTON

National Center for Atmospheric Research, Boulder, Colorado*

BENJAMIN D. SANTER

Program for Climate Model Diagnosis and Intercomparison, Livermore, California

WILLIAM D. COLLINS, JULIE M. ARBLASTER, AIXUE HU, DAVID M. LAWRENCE, HAIYAN TENG, LAWRENCE E. BUJA, AND WARREN G. STRAND

National Center for Atmospheric Research, Boulder, Colorado*

(Manuscript recieved 23 January 2005, in final form 17 June 2005)

ABSTRACT

Climate change scenario simulations with the Community Climate System Model version 3 (CCSM3), a global coupled climate model, show that if concentrations of all greenhouse gases (GHGs) could have been stabilized at the year 2000, the climate system would already be committed to 0.4°C more warming by the end of the twenty-first century. Committed sea level rise by 2100 is about an order of magnitude more, percentage-wise, compared to sea level rise simulated in the twentieth century. This increase in the model is produced only by thermal expansion of seawater, and does not take into account melt from ice sheets and glaciers, which could at least double that number. Several tenths of a degree of additional warming occurs in the model for the next 200 yr in the Intergovernmental Panel on Climate Change (IPCC) Special Report on Emissions Scenarios (SRES) B1 and A1B scenarios after stabilization in the year 2100, but with twice as much sea level rise after 100 yr, and doubling yet again in the next 100 yr to 2300. At the end of the twenty-first century, the warming in the tropical Pacific for the A2, A1B, and B1 scenarios resembles an El Niño–like response, likely due to cloud feedbacks in the model as shown in an earlier version. Greatest warming occurs at high northern latitudes and over continents. The monsoon regimes intensify somewhat in the future warmer climate, with decreases of sea level pressure at high latitudes and increases in the subtropics and parts of the midlatitudes. There is a weak summer midlatitude soil moisture drying in this model as documented in previous models. Sea ice distributions in both hemispheres are somewhat overextensive, but with about the right ice thickness at the end of the twentieth century. Future decreases in sea ice with global warming are proportional to the temperature response from the forcing scenarios, with the high forcing scenario, A2, producing an ice-free Arctic in summer by the year 2100.

1. Introduction

Multimember ensemble simulations using the Community Climate System Model version 3 (CCSM3), a global coupled climate model, have been conducted for 1) twentieth-century climate, 2) three scenario simulations to 2100 [using Intergovernmental Panel on Climate Change (IPCC) Special Report on Emissions Scenarios (SRES) A2, A1B and B1], and 3) stabilization experiments for concentrations of greenhouse gases (GHGs) stabilized at year 2000 values, and at year 2100 values for A1B and B1. These experiments have been performed by the global coupled climate modeling community for assessment for the IPCC Fourth Assessment Report (AR4) as described in Meehl et al. (2005a). The twentieth-century stabilization experiment was run out 100 yr, and the other two were run for an additional 200 yr to the year 2300. See section 2 for

* The National Center for Atmospheric Research is sponsored by the National Science Foundation.

Corresponding author address: Dr. Gerald Meehl, NCAR, P.O. Box 3000, Boulder, CO 80307.
E-mail: meehl@ncar.ucar.edu

more details on these experiments. The response of this model for these experiments was compared to a similar set of experiments performed with the Parallel Climate Model (PCM; Meehl et al. 2005b). Results from that comparison showed that changes to the thermohaline circulation in the Atlantic affected ocean heat uptake and sea level rise.

Earlier experiments for the twentieth century (e.g., Stott et al. 2000; Broccoli et al. 2003; Meehl et al. 2004a) have shown that the combination of natural and anthropogenic forcings are required to reproduce the time evolution of observed globally averaged surface temperatures. These experiments included anthropogenic forcings such as GHGs, ozone, and sulfate aerosol direct effects, as well as natural forcings such as volcanic aerosols and solar variability. Here, the CCSM3 includes those forcings as well as black carbon aerosols. The twentieth-century experiments provide a starting point for the twenty-first century scenario experiments as prescribed for assessment in the IPCC AR4 (e.g., Meehl et al. 2004b). These include three of the SRES scenarios for twenty-first century (A2, A1B, and B1), as well as stabilization experiments as described above.

In this paper we describe the suite of climate change experiments that have been performed with the CCSM3 and highlight some key results from these experiments. Where possible, we identify some of the physical processes responsible for the climate change responses in the model. Section 2 reviews the model characteristics and forcings, as well as the experimental design. Sections 3 and 4 give model results for global averages and geographical patterns, respectively. Section 5 discusses the summer drying results, section 6 addresses sea ice in the polar regions, a discussion is presented in section 7, and section 8 presents conclusions.

2. Model description and experimental design

The CCSM3 is a global coupled climate model descended from its predecessor version, the CCSM2 (Kiehl and Gent 2004). However, as described elsewhere in this issue (Collins et al. 2006a), a number of changes and improvements have been made to the CCSM3. In this paper we describe results from the T85 version of CCSM3, with grid points in the atmosphere roughly every 1.4° latitude and longitude, and 26 levels in the vertical, with the top two model hybrid level midpoints at 3.54 and 7.39 hPa. We mostly address climate changes near the earth's surface or in the upper layers of the ocean in this paper, so the resolution of the stratosphere and the location of the top level of the model do not appreciably affect the results here. The ocean is a version of Parallel Ocean Program (POP) with a nominal latitude–longitude resolution of 1° (1/2° equatorial Tropics) and 40 levels in the vertical, with Gent–McWilliams and *K*-profile parameterization (KPP) mixing. The land surface model is the Community Land Model (CLM), and the elastic–viscous–plastic (EVP) dynamic and thermodynamic sea ice component is the Community Sea Ice Model version 4 (CSIM4). No flux adjustments are used in the CCSM3.

The T85 version of CCSM3 was run for a present-day (1990) control run, as well as for a preindustrial (1870) control run. The latter was used as an initial state for the twentieth-century simulations. For the present-day control run, first the T85 atmosphere was tuned to near-zero (less than 0.1 W m^{-2}) net energy balance at the top of atmosphere using the same land mask as the coupled model and observed SSTs. The ocean was initialized with Levitus observations, whereas the sea ice and land surface conditions were initialized from a previous run with observed forcing. The components were then coupled and run for an initial 100-yr spin-up adjustment period where sea ice in the first few decades increased, then decreased, and became nearly stable after about 100 yr. At this time there was a small (about -0.2 W m^{-2}) net radiative imbalance at the top of atmosphere associated with a gradual cooling of the deep ocean. The present-day (1990) control was then run for 400 yr. The idealized forcing experiment with 1% yr^{-1} compound CO_2 increase was branched from this control simulation.

For the 1870 control run, a version of the model was formulated including an interactive sulfur cycle which increased the model run time about 20%, and a branch was run from the 1990 control run with GHGs and solar forcing instantaneously set to 1870 values. Sulfates were set to near zero. The model underwent an initial cooling, but after about 300 yr, the surface climate stabilized, with a net radiative imbalance of about -0.6 W m^{-2} at the top of atmosphere. This was associated with somewhat greater cooling in the deep ocean than in the 1990 control run. After the surface temperatures stabilized (i.e., long-term trend of -0.011°C $century^{-1}$), this 1870 control run was continued for another 400 yr. For the purposes of the climate change experiments to be analyzed shortly, we assume that the deep ocean cooling trend does not appreciably affect the surface climate change signals. The upper ocean in both control runs is relatively stable, and much of the climate change response in the coupled model occurs in the atmosphere and upper part of the ocean.

a. Twentieth-century simulations

The twentieth-century simulations run in the United States were started from different times in the 1870

control run separated by 20 yr with the first ensemble member branching from the control run at year 360 (as noted above this control run stabilized after about 300 yr, so these experiments started branching 60 yr after the control run showed a stable surface climate). The runs in Japan branched at 30- and 50-yr intervals from the control run there, so chosen to have different Atlantic meridional overturning initial states than the other ensemble members. The forcings included in the twentieth-century simulation are as follows.

Sulfate: direct effect from sulfur cycle model using time- and space-varying SO_2 emissions (Smith et al. 2001, 2004);
Solar: Lean et al. (1995);
Volcanoes: Ammann et al. (2003; volcanic effects included as aerosol optical depths);
Ozone: twentieth-century tropospheric ozone (up to tropopause defined by temperature gradient) spatially varying as computed from the Model for Ozone and Related Chemical Tracers (MOZART) model, snapshot runs every 20 yr: 1890, 1910, 1930, 1950, 1970, 1990 on T42 18L resolution with meteorology from PCM all-forcings twentieth-century run (Meehl et al. 2004a) for those years using spatially varying emissions of ozone precursors (Lamarque et al. 2005). Interpolation was then performed in space and time to the Community Atmospheric Model version 3 (CAM3) T85 26L. Time-varying zonal mean stratospheric ozone was prescribed from a National Oceanic and Atmospheric Administration (NOAA) dataset to 1990 (Kiehl et al. 1999). The top two model levels have exactly the zonal mean values. Levels to the tropopause are weighted and interpolated, and therefore contain some imprint from the tropopause (i.e., those levels are not purely zonal means). From 1990 to 2000, 1990 column tropospheric ozone has no appreciable trend so 1990 values were filled in to 2000. Time-evolving stratospheric ozone for 1990 to 2000 was scaled by NOAA ozone dataset.
GHGs ($C0_2$, CH_4, N_20): From the IPCC Third Assessment Report [TAR; $C0_2$ from the Integrated Science Assessment Model (ISAM)].
Halocarbons (including SF6): (Dai et al. 2001). We use direct CFC11 and equivalent CFC12 where equivalent is based on forcing, not on global warming potentials (GWPs).
Other aerosols: A present-day estimate of the spatial distribution and magnitude of black carbon was scaled by population so there are time-evolving values of black carbon over the twentieth century with a fixed pattern; sea salt and dust spatial distributions are held fixed throughout the twentieth century at year 2000 values (Collins et al. 2006b). Land surface characteristics are fixed at present-day values.

b. Twenty-first century simulations

Three twenty-first century SRES scenario simulations were performed for A2, A1B, and B1. These three scenarios represent a range of possible outcomes for the twenty-first century with low (B1), medium (A1B), and high (A2) emissions of GHGs. The A2 scenario was used by nine global coupled climate models for the IPCC Third Assessment Report (Cubasch et al. 2001)

Details of the forcings are as follows.

Ozone: After 2000, tropospheric 3D monthly patterns for year t same as year 2000 patterns but scaled by $Q(t)/Q(2000)$, where Q = global mean radiative forcing from the IPCC TAR and reproduced in Wigley et al. (2002). After 2000, stratospheric ozone recovers consistent with Montreal Protocol as in the NOAA dataset.
GHGs: As in SRES for A2, A1B, and B1.
Sulfates: A discontinuity arose at the year 2000 in the sulfate datasets. This was due to the SRES datasets for the future scenarios overpredicting sulfate amounts after 1990, such that switching from the relatively accurate historical datasets to the future datasets at the year 2000 resulted in a discontinuity. Therefore, new future scenario SO_x emission datasets were generated for each scenario. Anomalies of the future SO_x emissions versus the year 2000 SO_x values were created for each SRES scenario. These anomalies were added to the Smith year 2000 data. The anomaly was distributed across the two vertical levels in the same ratio as the values of the two vertical levels of the Smith year 2000 data, making sure emission did not go below zero anywhere. Sulfate data was generated for the following dates (year–month) and interpolated in time: 1990–07, 2000–01, 2000–07, 2010–07, 2020–07, 2030–07, 2040–07, 2050–07, 2060–07, 2070–07, 2080–07, 2090–07, 2100–07.

Since the corrections were done on a grid cell basis, this could result in negative values for emissions in some of the scenarios for some regions. These differences could be considered as initial conditions; for example, they did not reflect long-term changes in what emissions would be in 2100. Therefore, we added (on a grid cell basis) the difference between both year 2000 datasets, which made the year 2000 data continuous. Then we added 4/5 of that difference in 2010, 3/5 of the

difference in 2020, etc., and then from 2050 onward the SO_2 was identical to the SRES scenarios. In that way there were no negative values or regions with abnormally low emissions. We then created a two-level ratio of the difference that was the same as the ratio of each level of the historical data to 2000 data, to the total historical 2000 data, and then we applied the 4/5, 3/5, 2/5, 1/5 weighting of that to the SRES values from 2010 to 2100.

Thus, the emissions over most of the century were then identical to the SRES values. These future emissions are described by Smith et al. (2005).

Carbon aerosols: Geographical distributions are scaled by future SO_2 amounts instead of keeping carbon aerosols constant after year 2000. Carbon aerosol scaling datasets were generated for each scenario as:

$$f(\text{year } N) = SO_2 \text{ (year } N)/SO_2 \text{ (year 2000)},$$

where SO_2 is the globally averaged SO_2 value. Data were generated for the following dates (year–month) and interpolated in time: 2000–01, 2000–07, 2010–07, 2020–07, 2030–07, 2040–07, 2050–07, 2060–07, 2070–07, 2080–07, 2090–07, 2100–07. These values were created by using the sulfate inventories, globally integrated, and dividing by the year 2000 global integral;

Sea salt and dust: held at year 2000 values.

c. Stabilization (climate change commitment) simulations

Three stabilization experiments were carried out. In the first, concentrations of all atmospheric constituents were held fixed at year 2000 values (twentieth-century stabilization), and the model was integrated for 100 yr with these stabilized concentrations to assess how much climate change we are already committed to. That is, if we could have stabilized concentrations at the year 2000, how much more additional climate change would occur over the next 100 yr? The idea of committed warming was described by Ramanathan (1988), and has been elaborated on since, for example, with simple models (Wigley 2005). Here we quantify not only globally averaged but regional climate change commitment with a global coupled climate model.

In the other two stabilization experiments, all concentrations for the A1B and B1 simulations were held fixed at year 2100 values, and the model was integrated to the year 2300. In this way we can assess how much additional climate change would occur if we could stabilize concentrations at year 2100 in two different SRES scenarios. (Note that Fig. 3a illustrates the various experiments by showing CO_2 concentrations for the three SRES scenarios and the three stabilization scenarios.)

d. Ensembles

Eight-member ensembles of the CCSM3 were run for the twentieth century and for each scenario (except twentieth-century stabilization and A2 where there were five), with the considerable computational burden required for five of the ensemble members spread between a number of supercomputer centers in the United States [National Center for Atmospheric Research (NCAR), Oak Ridge National Laboratory (ORNL), and the National Energy Research Scientific Computing Center (NERSC)]. All of these were run on IBM supercomputers, with the machines at NCAR and ORNL being identical IBM Power-4 architectures. Porting the CCSM3 from NCAR to the earlier model (Power-3) IBM at NERSC involved carrying out matching control runs at each site to verify that the model code produced climatologically identical answers. Ensemble members were started and finished on the same machines. Consequently, no experiment was transferred to a different machine in the middle of a run. These experiments in the United States were supplemented by three additional ensemble members (except for A2) that were run on the Earth Simulator in Japan. A similar procedure to verify a successful model port was done on the Earth Simulator. In addition to the three ensemble members for each scenario (except A2), there were further runs performed to address more scenarios of future climate change (Yoshida et al. 2005). Here we show results for the eight-member ensemble (except for five for twentieth-century stabilization and A2) including the CCSM3 runs performed in the United States and Japan.

e. Climate sensitivity and factors contributing to the response

The CCSM3 has somewhat higher sensitivity than earlier versions of PCM and CCSM2, with an equilibrium climate sensitivity of 2.7°C and transient climate response (TCR; defined as the globally averaged surface temperature difference at the time of CO_2 doubling in a 1% yr^{-1} CO_2 increase experiment; e.g., Cubasch et al. 2001) of 1.5°C. For comparison, the PCM has an equilibrium sensitivity of 2.1°C and a TCR of 1.3°C, and CCSM2 has an equilibrium climate sensitivity of 2.2°C and a TCR of 1.05°C (Meehl et al. 2004c). A detailed discussion of various aspects of climate sensitivity and TCR is included in this volume (Kiehl et al. 2006). The meridional overturning maximum in the North Atlantic in the preindustrial control run for CCSM3, indicative of the thermohaline circulation in

the ocean, is 21.9 Sv (Bryan et al. 2006). This is weaker than some earlier model versions (CSM1 was about 30 Sv, PCM was 32.1 Sv; Meehl et al. 2004c) but stronger than in CCSM2 (15.7 Sv; Gent and Danabasoglu 2004). This is relevant since the mean strength of the meridional overturning and its changes are an indication of ocean ventilation and contribute to ocean heat uptake and consequent time scales of temperature response in the climate system (Meehl et al. 2004c; Gent and Danabasoglu 2004). A comparison of the responses of CCSM3 and PCM for these 1PCC experiments is given by Meehl et al. (2005b).

3. Globally averaged results

Figure 1a shows the globally averaged surface air temperature anomaly time series for the CCSM3 compared to observations. The warming during the twentieth century in CCSM3, 0.7°C averaged over the period 1980–99, is close to the observed for that same time period of 0.6°C (Folland et al. 2001a). The time evolution of the globally averaged surface air temperature is also similar to the observations, with increases of temperature occurring in the first half of the twentieth century, a flattening out in the 1950s and 1960s, and a greater rate of warming after the late 1970s. This similarity to the observations has been shown to be due to a combination of natural and anthropogenic forcings acting on the climate system during the twentieth century (Stott et al. 2000; Broccoli et al. 2003; Meehl et al. 2004a). However, it is interesting to note that in the CCSM3, the peak of warming that occurred in the observations in the mid-1940s is delayed somewhat to the late 1950s. This was not seen in an earlier version of PCM (Meehl et al. 2004a). However, the PCM used a different version of solar forcing (Hoyt and Schatten 1993) compared to CCSM3 (Lean et al. 1995), and these solar forcing reconstructions have different time evolving characteristics.

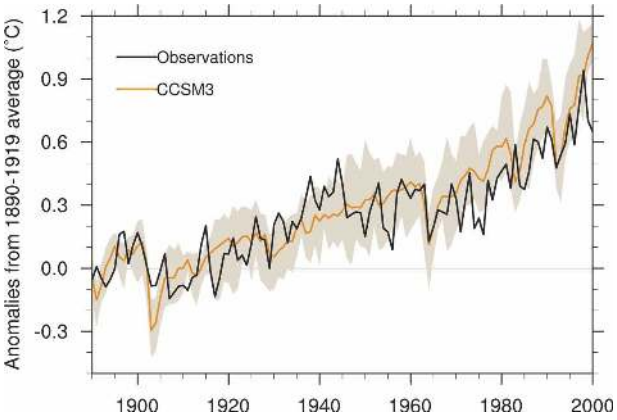

FIG. 1. Time series of globally averaged surface air temperature anomalies (°C) for the twentieth century from the CCSM3 compared to observations (black line; Folland et al. 2001b). Shading indicates the range of ensemble members. Solid colored line is the ensemble mean of the eight-member ensemble.

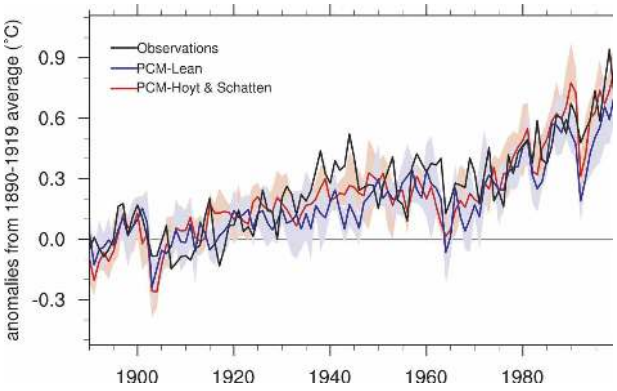

FIG. 2. Time series of globally averaged surface air temperature anomalies (°C) from simulations with the PCM showing the effects of two different solar forcing datasets (Hoyt and Schatten 1993 vs Lean et al. 1995). Light shading depicts range of the five-member ensembles, solid colored lines are ensemble means, and solid black line is observations (Folland et al. 2001b). Anomalies are calculated relative to the 1890–1919 base period.

To gain insight into how the time-evolving characteristics of globally averaged temperatures in CCSM3 could be affected by the use of a particular solar forcing dataset, we performed ensemble experiments with the PCM using the Lean et al. solar forcing that is used in CCSM3, and compared those results to the earlier PCM simulation with Hoyt and Schatten solar forcing (Meehl et al. 2004a). This experiment could be performed readily with the PCM with minimal computational cost at T42 thus leveraging the earlier suite for forcing experiments with the PCM to gain insight into the behavior of CCSM3. These experiments used multiple natural and anthropogenic forcings (see Meehl et al. 2004a), but the only difference between the two ensembles is that one uses the Hoyt and Schatten (1993) solar forcing, and the other uses Lean et al. (1995). Figure 2 shows that simply by changing the solar forcing dataset, the experiment using the Hoyt and Schatten solar forcing shows a peak of globally averaged temperatures in the mid-1940s, similar to when the peak in the solar forcing occurred, while the experiment using Lean et al. peaks in the 1950s as does the solar forcing. The latter is closer to the CCSM3 simulation in Fig. 1.

There is a degree of uncertainty regarding these different solar forcing reconstructions (e.g., Foukal et al. 2004) that is reflected in the climate model simulations. That is, Foukal et al. (2004), Lean et al. (2002), and others have questioned the earlier solar reconstructions of Hoyt and Schatten (1993) and Lean et al. (1995) in

that low-frequency variation of solar output may be manifested only as amplitude modulation of the 11-yr solar cycle. This could reduce the amplitude of the low-frequency solar forcing that was present in the earlier reconstructions. We are currently performing sensitivity experiments with solar forcing that includes only amplitude modulation of the 11-yr solar cycle. Preliminary results show that the early century warming in the coupled model still occurs, but with somewhat reduced amplitude.

Figure 3a shows time series of CO_2 concentrations for the different experiments as described above. The response of the CCSM3 to these concentrations and the other forcings included in the model (also described above) is shown in Fig. 3b, which is the time series of globally averaged surface air temperature anomalies for the various experiments extending from the twentieth century to the year 2300. Anomalies are computed relative to a 1990–2009 multimember ensemble average.

Figure 3c shows globally averaged time series of sea level rise anomalies from thermal expansion. Note that sea level change is calculated offline (after the model integration is done) and includes both thermal-steric and halosteric changes, but is dominated by thermal-steric (thermal expansion) changes. In CCSM3's ocean component, a free surface is employed, and these changes to the free surface are included in the sea level calculation, but there is no water mass exchange between air and sea. Instead, the air–sea freshwater exchange is parameterized by a virtual salt flux, and the total water volume of the ocean does not change during the model run. Therefore, although the salinity of seawater changes with time due to the changes of freshwater flux into the ocean, its effect on sea level change may have been underestimated by the current model setup. Consequently, the sea level calculation is dominated by thermal expansion of the water column. The sea level anomalies are calculated relative to the long-term mean of the control run (a 200-yr period), and then the linear trend of the control run is removed from each run.

Over the period of the twentieth century, sea level in the CCSM3 rose 4.7 cm by the year 1999. The observed estimate for this time period is 15–20 cm (Miller and Douglas 2004; Church et al. 2004). The lower value from the model is consistent with the part of twentieth-century warming thought to be caused by thermal expansion (Miller and Douglas 2004) because as the ocean warms, seawater expands, and sea level rises. This study estimates that roughly a third of the observed sea level rise in the twentieth century was likely due to thermal expansion. Thus, the CCSM3 is on the

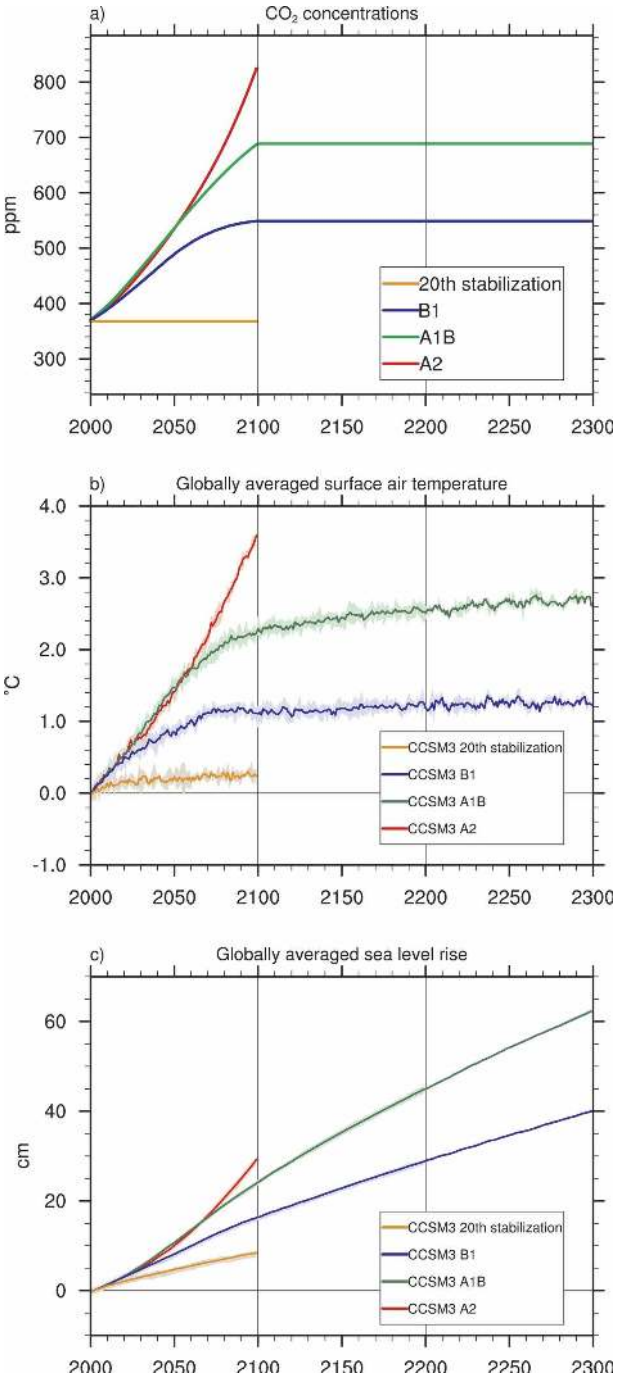

FIG. 3. (a) Time series of CO_2 concentrations (ppm) for scenarios B1, A1B, and A2, twentieth-century stabilization from 2000 to 2100, twenty-first century stabilization from 2100 to 2300 for B1 and A1B; (b) time series of globally averaged surface air temperature anomalies (°C), 2000–2300, for the various experiments; (c) same as (b) except for globally averaged sea level anomalies from thermal expansion (cm).

low end of these estimates, but still well within the uncertainties of the observations. Additionally, Barnett et al. (2005) have shown that a current global coupled climate model that is a predecessor of the CCSM3, the PCM, shows about the right warming as a function of depth and basin, indicating that the thermal expansion values for sea level rise in the current model are probably at least relatively close to the observed estimates.

The CCSM3, however, does not include contributions to sea level rise due to ice sheet or glacier melting. Thus, the simulated sea level rise is at least a factor-of-2 too small compared to observed estimates. Therefore, the CCSM3 results should be considered the minimum values of sea level rise and also can provide a general indication of ocean heat uptake processes related to sea level rise and climate change commitment over time.

If we could have stabilized concentrations of all atmospheric constituents from any further increases in the year 2000, the CCSM3 indicates we are already committed to 0.4°C more global warming by the year 2100 compared to 0.6°C observed warming realized by the end of the twentieth century (Fig. 3b).

Note that the range of the ensembles for the climate model temperature anomalies here is about ±0.1°C. This spread among the ensemble members for the temperature (and sea level rise values that are described below) is mainly due to the different initial conditions at the start of the various ensemble members. Inherent variability of the coupled system produces the different initial states, and the resulting simulations take somewhat different tracks as a consequence.

We are already committed to proportionately much more sea level rise (Fig. 3c), with about a 200% increase from thermal expansion compared to the values cited above for ensemble mean sea level rise at the year 1999. This result has been shown before in various other contexts (e.g., Wetherald et al. 2001; Stouffer and Manabe 1999; Mitchell et al. 2000; Wigley and Raper 2003; Wigley 2005), but is reinforced and well-illustrated with this large number of ensemble simulations from the CCSM3.

The low estimate climate change scenario (SRES B1) shows a warming in the CCSM3 by mid-twenty-first century compared to the end of the twentieth century of 0.9°C (Fig. 3b), with an additional sea level rise of 8 cm (Fig. 3c). Note that the spread among the ensembles for sea level for all cases amounts to less than ±0.3 cm for reasons mentioned above with regards to temperature. At the end of the twenty-first century compared to end of twentieth century values, the warming has increased to 1.2°C for the CCSM3, with sea level rising to 17 cm above year 1999 levels. A medium-range scenario (SRES A1B) produces a warming at the middle of the twenty-first century compared to the end of the twentieth century of 1.1°C, and a sea level rise of 11 cm. By the end of the twenty-first century, there is a warming in this scenario of 2.3°C with about 25-cm sea level rise. For the high estimate scenario (A2), ensemble mean warming at 2100 is 3.3°C, and sea level rise is 31 cm. Note that by 2050, there is little difference between the high- and medium-range scenarios, and only a few tenths of a degree Celsius difference with the low scenario. Subsequently, there is more spread among the scenarios so that the differences are larger and more readily differentiated from each other by 2100.

If concentrations of all greenhouse gases in these simulations are held fixed at year 2100 values, we would be committed to an additional warming by the year 2200 for B1 of about 0.2°C (Fig. 3b). This small warming commitment is related to the fact that CO_2 concentrations had already started to stabilize at about 2050 in this scenario (Fig. 3a). But even for this small warming commitment in B1, there is almost double the sea level rise seen over the course of the twenty-first century by 2200, or an additional 13 cm (Fig. 3c). For A1B, there is 0.44°C additional warming by 2200, but again there is roughly a doubling of twenty-first century sea level rise by the year 2200, or an additional 21 cm. By 2300, with concentrations still held at year 2100 values, there would be less than another 0.1°C warming for either scenario, but yet again about another doubling of the committed sea level rise that occurred during the twenty-second century, with additional increases of 18 cm from thermal expansion for the stabilized B1 experiment, and 21 cm for A1B compared to year 2200 values. Note that at 2300, the sea level rise values are still increasing, implying sea level rise commitment well into the future (e.g., Wigley 2005).

Time series of ocean heat uptake for the upper 300 m and upper 3000 m are shown in Figs. 4a,b, respectively. The changes in sea level in Fig. 3c are manifested in the increases of upper 3000-m ocean heat uptake, with heat content increasing over time in proportion to the sea level rise from thermal expansion. The upper 300-m heat content is closely related to the surface temperature time evolution in Fig. 3b, showing more of a leveling off of heat content in the commitment experiments. The upper 3000-m heat content change is about 16.5×10^{22} J, and is equivalent to a 0.42°C increase in ocean temperature, which is very close to the observed changes (14.5×10^{22} J and 0.37°C; Levitus et al. 2005). About 50% of this heat content increase is due to the warming of the upper 300 m of the ocean, amounting to about 0.2°C, and this also agrees well with the observations. At 2100, the heat content of upper 300 m increases by an additional 18, 39, 63, and 85×10^{22} J, and

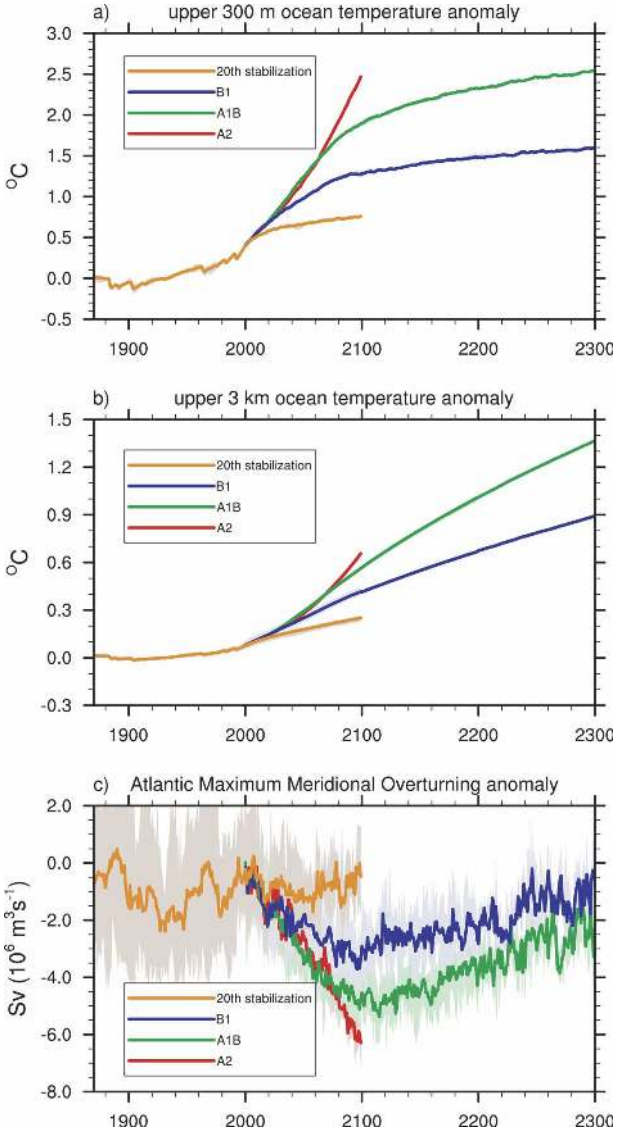

FIG. 4. (a) Heat uptake (vertically averaged temperature, °C) for upper 300 m, 1870 to 2300; (b) same as (a) except for upper 3 km; (c) Atlantic meridional overturning circulation (Sv), 1870–2300. The potential temperature changes in (a) and (b) can be converted to heat content anomalies by multiplying $\rho_0 CpV$, where ρ_0 is the reference water density, Cp is the specific heat of seawater, and V is the volume of the model ocean. In the model, $\rho_0 Cp$ is a constant and equal to 4.1×10^6 J °C^{-1} m^{-3} and the volumes of seawater in upper 300 m and upper 3 km are 0.1 and 0.947×10^9 km^{-3}, respectively.

in the upper 3000 m the increases are 70, 133, 188, 220 $\times 10^{22}$ J for, respectively, the twentieth century commitment, B1, A 1B, and A2 experiments relative the mean value of 1995–1999. Ocean heat uptake in the CCSM3 twentieth-century simulation is discussed in this volume by Gent et al. (2006).

Time series of meridional overturning circulation (MOC) in the North Atlantic are shown in Fig. 4c. First the linear trend from the control run is removed from the MOC time series, and then anomalies are computed in relation to the long term means. The CCSM3 at 2100 for the B1, A1B, and A2 scenarios shows decreased MOC in the North Atlantic (−4.0, −5.3, and −6.2 Sv or −18%, −24%, and −28%, respectively). The MOC in the twenty-first century after concentrations are stabilized continues to weaken slightly and then shows a modest recovery to nearly the values of the year 2000. For the stabilization experiments for A1B and B1, the MOC recovers gradually over the next two centuries.

The processes that contribute to the warming commitments involve small radiative flux anomalies at the surface (differences on the order of several tenths of a W m^{-2} compared to the preindustrial control) after atmospheric GHG concentrations are stabilized. These small net heat flux anomalies into the ocean are transferred to the deeper layers through mixing and ventilation processes such as the meridional overturning circulation that connects the Northern and Southern Hemisphere high-latitude deep ocean circulations (Hu et al. 2004). Further details of meridional overturning in CCSM3 are given in this volume by Bryan et al. (2006). Thus, in addition to changes in the meridional overturning circulation, the strength of the mean circulation also plays a role (Raper et al. 2002; Stouffer 2004; Meehl et al. 2004c).

4. Geographic patterns of climate change

Geographic patterns of temperature change (Fig. 5) for A1B show larger warming at high northern latitudes and over land, and geographic temperature increases roughly proportional to the amplitude of the globally averaged temperature increases in the different scenarios (A1B is shown to illustrate the similar patterns in the other scenarios, with the amplitude of the pattern proportional to the forcing as represented for CO_2 in Fig. 3a). Note that the slow-down in meridional overturning in the CCSM3 does not result in less warming over northern Europe. The warming from increases of GHGs overwhelms any tendency for widespread decreased high-latitude warming from less northward heat transport by the weakened meridional overturning circulation in the Atlantic, though the relative minimum of warming in the North Atlantic is related to weakened meridional overturning and associated changes in ocean currents in that region (Hu et al. 2004; Dai et al. 2005). Note the El Niño–like response (Meehl and Washington 1996) in the equatorial Pacific in CCSM3, with greater warming in the near-equatorial central and eastern Pacific. This response has previ-

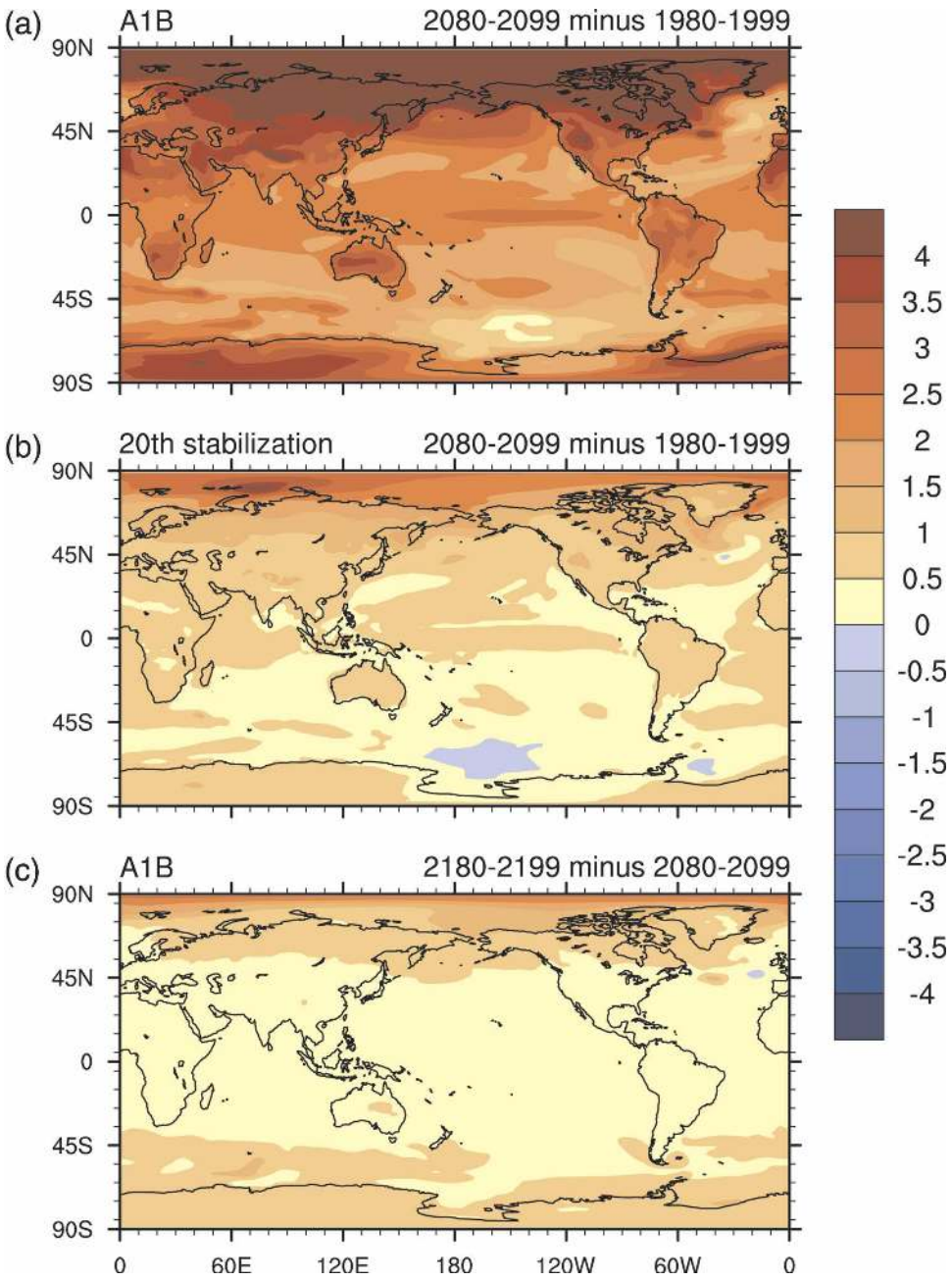

FIG. 5. (a) Geographic plots of annual mean surface air temperature differences (°C) for A1B scenario, 2080–99 minus 1980–99; (b) same as (a) except for twentieth-century stabilization experiment; (c) same as (b) except for twenty-first-century stabilization experiment, 2180–99 minus 2080–99.

ously been attributed to cloud feedbacks involving the prognostic cloud liquid water scheme, such as the one included in the CCSM3, compared to the diagnostic cloud liquid water formulation in the CSM1 where there is no El Niño–like response (Meehl et al. 2000).

The pattern of warming commitment from the twentieth-century stabilization experiments (Fig. 5, bottom) shows the same type of pattern in the forced experiments, with greater warming over high latitudes and land areas. It is worth noting that for regions such as much of North America, we are already committed to more than an additional half a degree warming. The pattern of temperature change in the twentieth-century stabilization experiment is similar to that produced in the twenty-first century stabilization experiments with A1B and B1 (not shown).

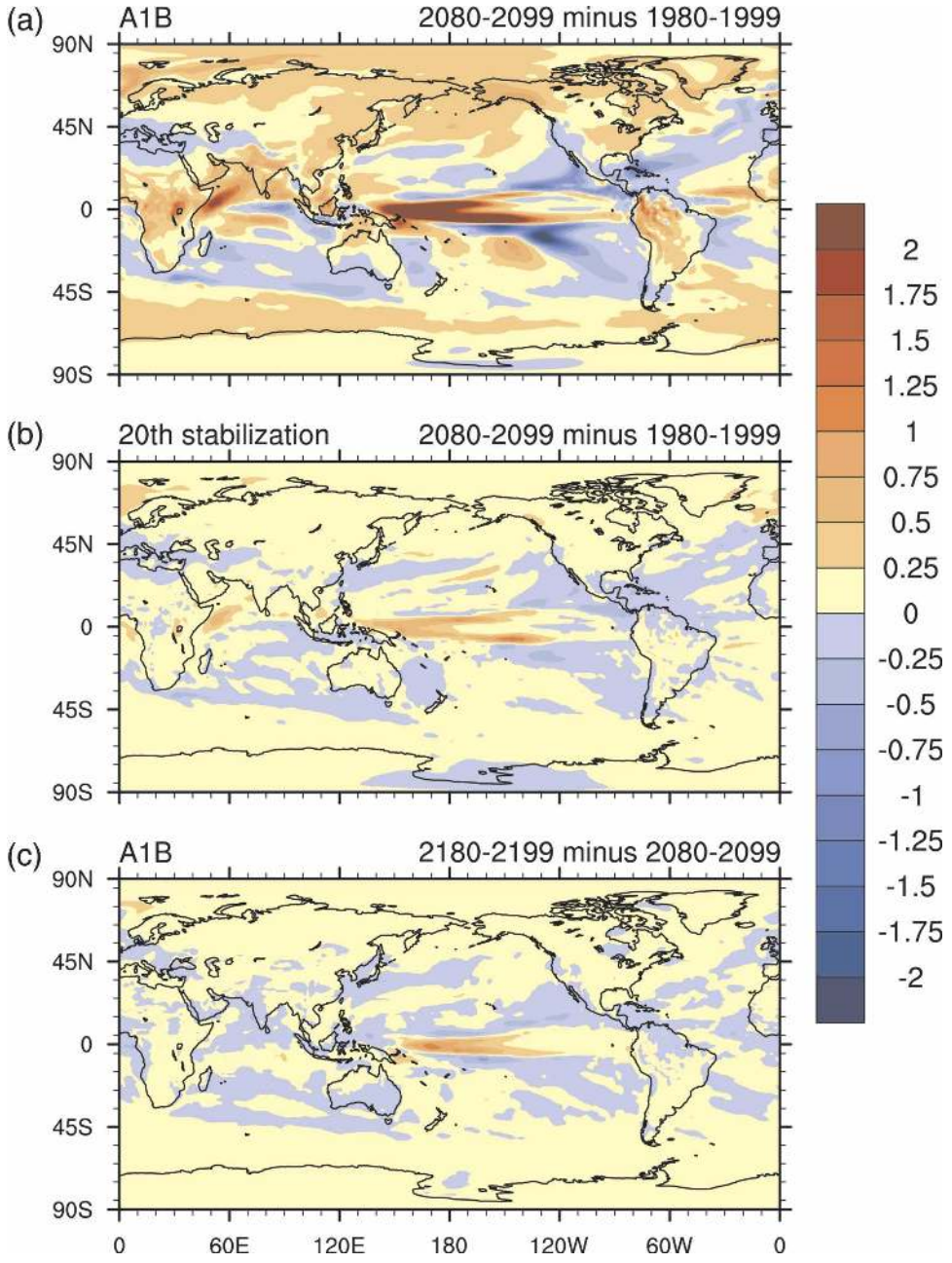

FIG. 6. (a) Same as Fig. 5a except for annual mean precipitation differences (mm day^{-1}); (b) same as Fig. 5b except for precipitation differences; (c) same as Fig. 5c except for precipitation differences.

Figure 6 shows geographical distributions of precipitation differences, again for the A1B scenario, at the end of the twenty-first century as in Fig. 5. Generally, precipitation increases in the Tropics (particularly over areas of the tropical Pacific associated with the El Niño–like response mentioned above in reference to Fig. 5), decreases in the subtropics, and increases again in the midlatitudes consistent with a multimodel ensemble mean of previous models used in the IPCC TAR (e.g., Cubasch et al. 2001). Note that the monsoon regimes in the South Asian, West African, and South American regions show increases in precipitation, also consistent with earlier results (e.g., Cubasch et al. 2001). The differences for the two commitment experiments (Figs. 6b,c) show lower amplitude and less consistent changes, particularly at the high southern latitudes for the twenty-first century commitment experiment in Fig. 6c. This is related in part to the smaller

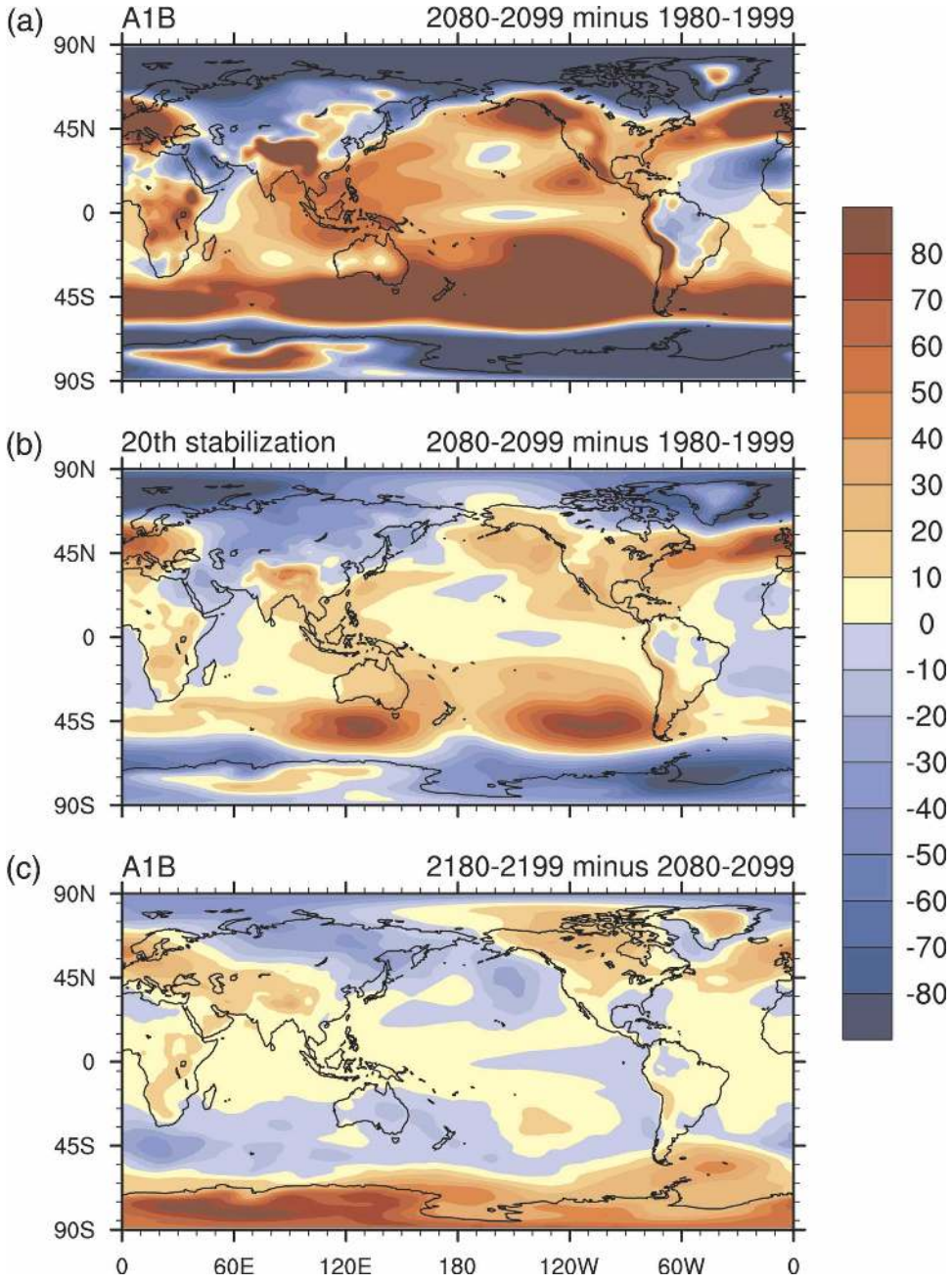

FIG. 7. (a) Same as Fig. 5a except for annual mean sea level pressure (SLP) differences (Pa); (b) same as Fig. 5b except for SLP differences; (c) same as Fig. 5c except for SLP differences.

signal and greater noise that characterizes precipitation anomaly patterns.

The changes in sea level pressure (SLP) are shown in Fig. 7 again for A1B at the end of the twenty-first century as in Figs. 5 and 6. These are annual mean differences, but it should be noted that a similar but higher amplitude pattern in the mid- and high latitudes occurs in the respective winter hemispheres (not shown). Associated with the El Niño–like response in SSTs in the tropical Pacific, the SLP differences in the Tropics also show an El Niño–like pattern with negative differences over the central equatorial Pacific and positive differences over the Eurasian region. There are also negative differences in the regions of the North and South Pa-

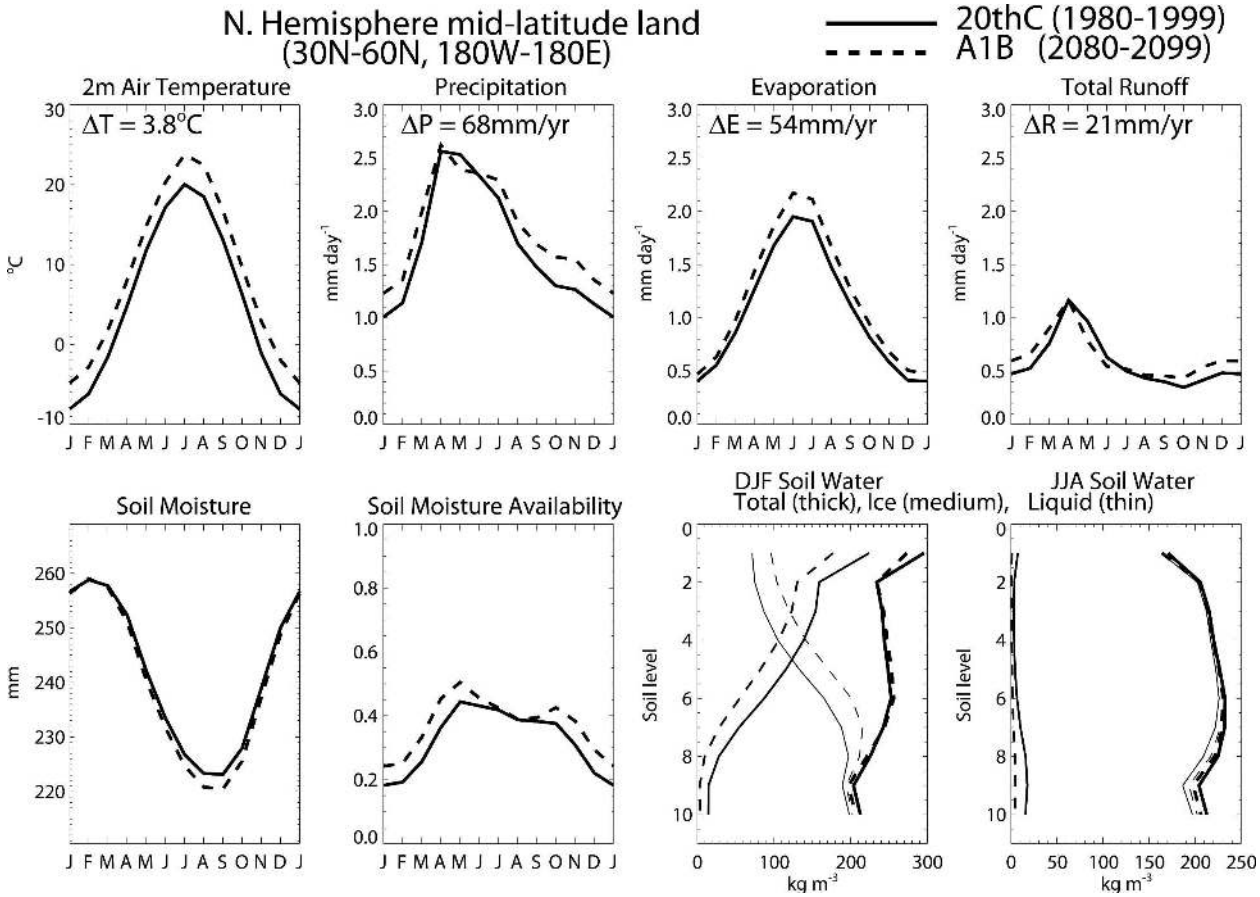

FIG. 8. Comparison of 20-yr mean annual cycles of the water budget for twentieth century (1980–99) and A1B (2080–99) ensemble means. Evaporation is sum of soil evaporation, transpiration, and canopy evaporation. Total runoff is sum of surface runoff and subsurface drainage. Soil moisture availability is a factor involved in the computation of transpiration that integrates soil wetness in each soil level with the root density profile (low values indicate high soil moisture limitation on transpiration). Soil moisture is total of unfrozen and frozen soil water for the top seven soil levels (0.62 m).

cific troughs consistent with the El Niño–like SST pattern. Negative SLP differences are also seen at high latitudes, and in the Southern Hemisphere this has the signature of an intensification of the Southern Annular Mode that has been attributed in earlier studies to be the response of the high southern latitudes to changes in stratospheric ozone and an increase in GHGs (e.g., Arblaster and Meehl 2006). In the CCSM3 IPCC scenarios, the Arctic Oscillation (AO) index shifts to the positive phase at the end of the twentieth century, but the increase is smaller compared to the observations (Teng et al. 2006a). Lack of the AO upward trend in models compared to observations has been a common feature among some current atmosphere–ocean general circulation models (AOGCMs), and understanding the relationship between AO and climate change is complicated by several issues that are beyond the scope of this paper (see Gillett et al. 2003).

5. Summer soil drying

A number of studies have indicated that midlatitude continental summer drying may be a significant consequence of global warming (Wetherald and Manabe 1995, 2002; Gregory et al. 1997; Cubasch et al. 2001) and that the increased drying may lead to an increased risk of summer midlatitude drought (Easterling et al. 2000). Other investigations suggest that the problem may not be as acute as reported in those studies due to systematic midsummer model dry biases and inadequate representation of the land surface in those models (Seneviratne et al. 2002). The impact of warmer climatic conditions under greenhouse forcing on the CCSM3 the soil moisture budget is briefly assessed here.

Figure 8 compares the mean water budget annual cycle for the Northern Hemisphere midlatitudes (30°–

70°N) for 20-yr time averages at the end of the twentieth century and, for A1B, the twenty-first century. For both periods, the mean annual water budget is approximately balanced and the annual mean total soil moisture content shows no obvious trends in either period. Total input of water into the soil (rainfall, strictly throughfall, plus snowmelt minus surface runoff) is about 0.2 mm day^{-1} larger at the end of the twenty-first century compared to the end of the twentieth century from October through March, but is roughly unchanged during the late spring and summer months. Rainfall itself is nearly uniformly heavier throughout the year by about 0.2–0.3 mm day^{-1}, but this is offset during the late spring and early summer by less snowmelt brought about by reduced winter snowfall. Warmer surface temperatures lead to stronger evaporation throughout the year. The changes in runoff largely follow the changes in water flux into the soil.

Late summer soils are slightly drier at the end of the twenty-first century compared to the end of the twentieth century due to stronger evaporation during late spring and early summer coupled with a relatively small difference in soil water input during those months (Fig. 8). During the fall and winter, however, soil moisture is replenished at a faster rate in the A1B run because of heavier precipitation. By late winter, the soils are actually wetter in the A1B run. To a certain extent, results from CCSM3 support the idea put forth by the previous studies mentioned above that there may be some midlatitude continental summer drying in a warmer climate, although the amplitude of the drying is relatively small in CCSM3.

However, the annual cycle of soil moisture availability, a parameter that integrates soil wetness with root density throughout the soil column and represents the soil moisture constraint on transpiration, indicates that the weak soil moisture drying seen in summer is not associated with a greater soil moisture stress on vegetation. Global maps show that over most of the Northern Hemisphere high latitudes, summer soil moisture stress is actually lower in the A1B runs (not shown). The only location exhibiting a notable increase in summertime soil moisture stress is over Europe where the model also predicts a significant midsummer rainfall reduction. The somewhat counterintuitive behavior of reduced soil water content corresponding to less soil moisture stress is due to the fact that soil liquid water content actually increases slightly at the expense of soil ice water content (see bottom right panels of Fig. 8). Outside of the summer season, thawing of soil ice water is even more distinct with Northern Hemisphere midlatitude total ice water content reduced by 7% in December–January (DJF).

It should be noted that soil moisture at depth (between 1 and 3 m deep) is uniformly drier throughout the year at the end of the twenty-first century. The small-amplitude deep soil drying is likely related to the reduction in soil ice water content and an associated modest increase in subsurface drainage that is a result of the larger amount of freely draining liquid water. The reduction in soil water ice content reflects the reduction of permafrost in mid- and high latitudes, a consequence of climate change that is likely to have a profound impact on ecological systems in those areas (Lawrence and Slater 2005).

6. Sea ice in the polar regions

Seasonal sea ice concentration from CCSM3 is compared with the Hadley Centre Sea ice and sea surface temperature (HadISST) observations (Rayner et al. 2003) over the years 1979–99, during which HadISST is mainly derived from satellite passive-microwave sensor measurements. For the Arctic (Fig. 9), the CCSM3 simulates sea ice distributions comparable to the observations, with somewhat too much sea ice in the Labrador Sea, and a bit less than observed north of Norway during the winter season. For summer the ice distributions are also close to observed, with somewhat less ice than observed north of Siberia. For the Antarctic in Fig. 10, the general characteristics of the sea ice distributions between CCSM3 and observations are similar, with the model simulating overextensive sea ice. The amplitude of the decreasing trends of Arctic and Antarctic area-averaged sea ice is similar to that observed for the latter part of the twentieth century (Teng et al. 2006a).

Most observational records of sea ice thickness are measured by upward-looking sonar from Scientific Ice Expeditions (SCICEX) cruises (data available online at www.nsidc.org), which roughly followed 150°W from the North Pole to the Beaufort Sea. Figure 11 shows SCICEX mean draft from the four available summers (SCICEX-93, -96, -97, and -98), along with model simulations for the same seasons. The symbols denote SCICEX data, and the lines are August–September mean sea ice thickness at 150°W for those same 4 yr averaged over the eight-member CCSM3 ensemble. There is good agreement between the observed and model sea ice thickness values for this measure.

For the climate change simulations with CCSM3, there is a continuous decrease of sea ice in both polar regions in the twenty-first century. The time series of seasonal mean sea ice extents are shown in Fig. 12 from 1979–2000 for the CCSM3 simulation and from 1979–2002 for the observations (Parkinson et al. 1999). The model output includes a time period in the twentieth

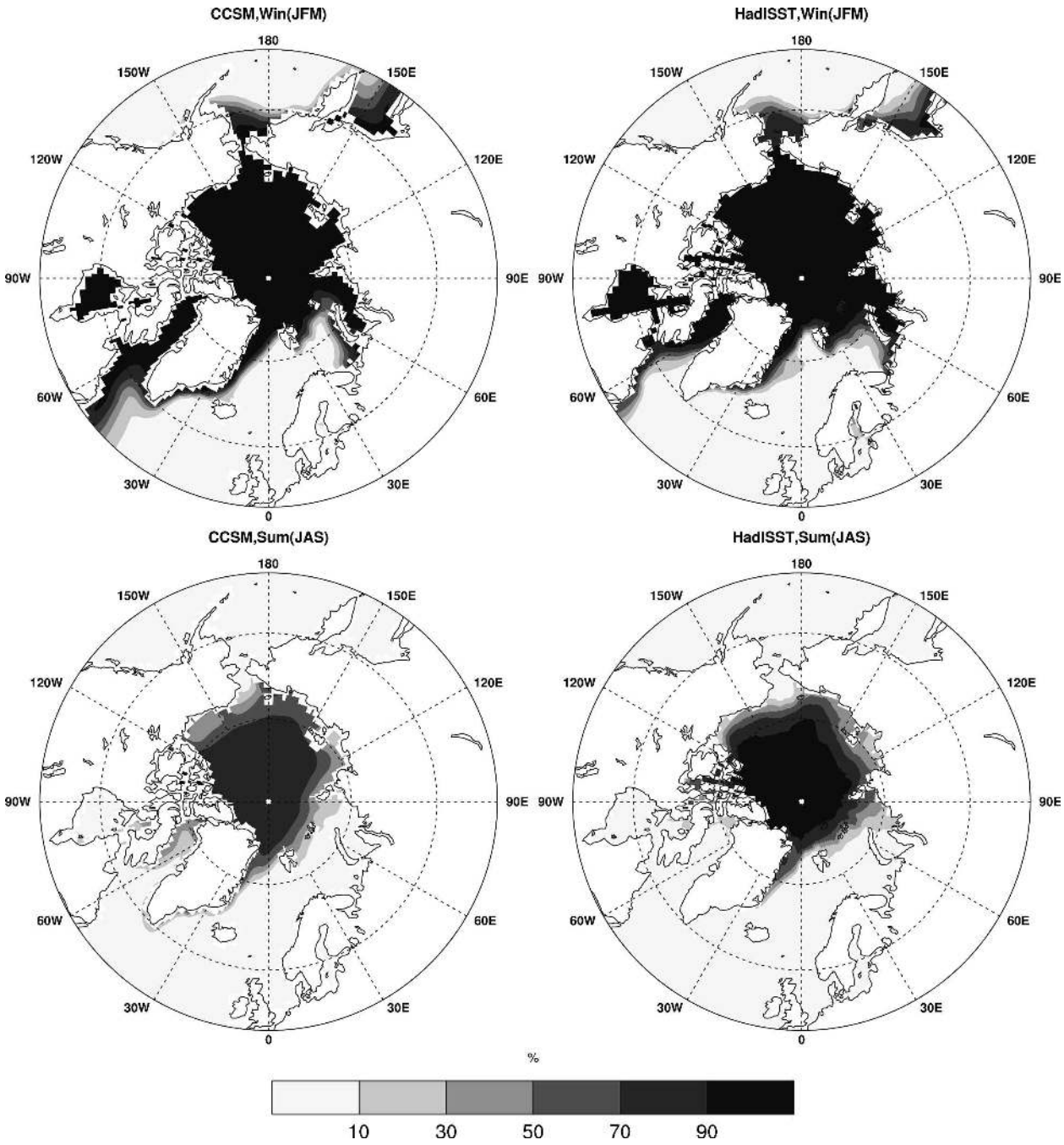

FIG. 9. Northern Hemisphere seasonal (JFM and JAS) sea ice concentrations (%) over the years 1979–99. (left) The model outputs are eight-member ensemble means from CCSM3 historical runs. (right) The observations are derived from HadISST.

century simulations from 1979–2000, and values for the A2 and B1 runs during 2000–2099. Arctic winter [January—March (JFM)], Arctic summer [July–September (JAS)], Antarctic summer (JFM), and Antarctic winter (JAS), all show that the model simulates greater than observed average ice extents. This was reflected in the geographical plots in Figs. 10 and 11. The decreases in ice extent are proportional to the warming in Fig. 3, with B1 losses in ice starting to level out by 2100, and greater decreases of ice in A2. Of interest in Fig. 12b is the JAS season in the Arctic that shows the closest agreement with observations, and also shows that, for

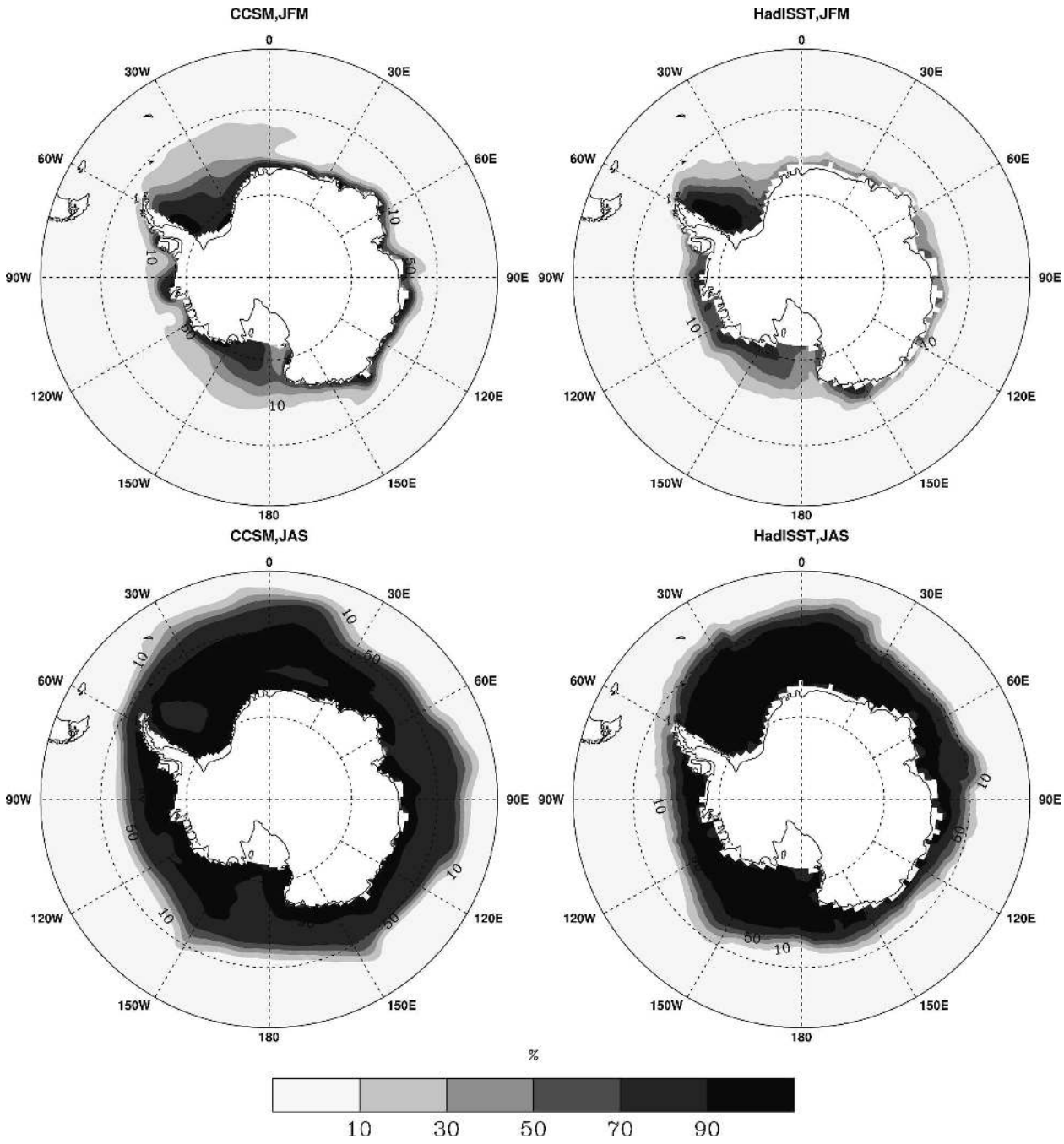

FIG. 10. Same as Fig. 9 but for the Antarctic.

the A2 scenario by the end of the twenty-first century, the Arctic is essentially ice free during summer.

7. Discussion

Recovery of the MOC with large forcing has been addressed in previous experiments (e.g., Stouffer et al. 2006; Hu et al. 2004). With very large forcing (4×CO2) in one experiment, the MOC did not recover over the time scale of several centuries (Manabe and Stouffer 1999). In all the experiments described here, the MOC recovers, and the rate of recovery affects the time scale of the climate change commitment (e.g., Meehl et al. 2005b). They showed that the PCM, with a larger mean MOC, less reduction in MOC with increased GHGs, and a quicker MOC recovery, had less climate change

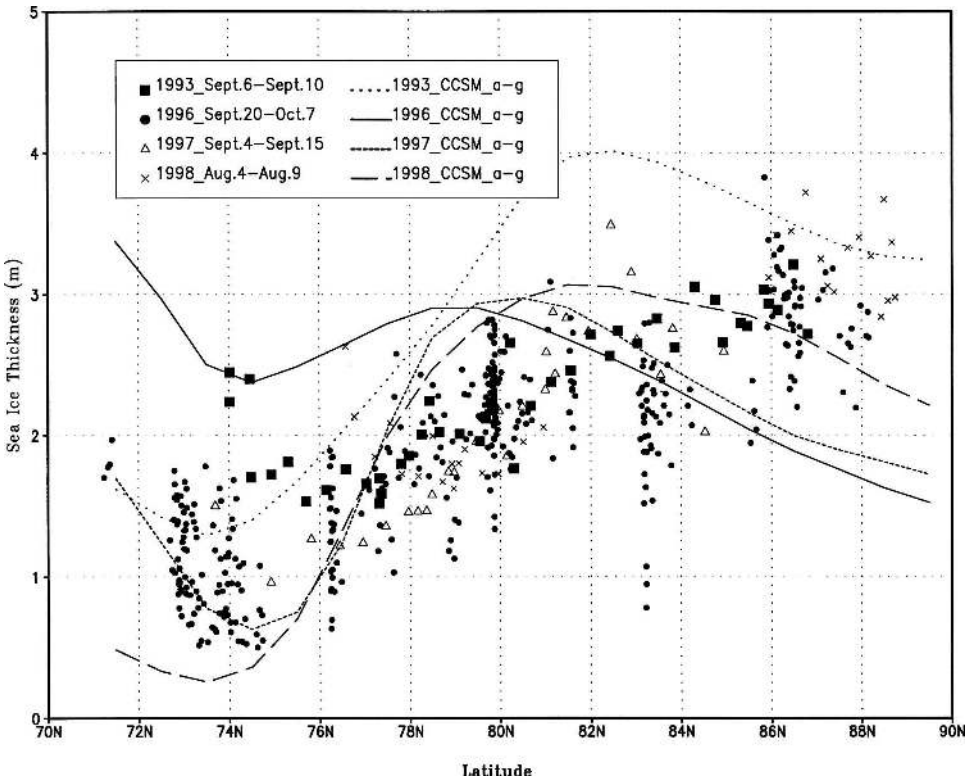

FIG. 11. Arctic sea ice thickness (m) along 150°W from 70° to 90°N. The symbols denote mean sea ice draft from SCICEX submarine observations (SCIEX-93, -96, -97, -98; refer to www.nsidc.org for data description). The lines are August–September mean sea ice thickness at 150°W in the same four years from CCSM eight-member ensemble means.

commitment than the CCSM3 with a smaller mean MOC, a longer time scale of MOC recovery, and a greater climate change commitment. The fact that the MOC recovers on the time scale of these experiments and for these forcings does not mean more severe MOC effects could be experienced with greater forcing (e.g., an A2 commitment experiment or SRES A1FI).

The relationship between changes in sea level pressure and indices of the North Atlantic Oscillation (NAO, or the Arctic Oscillation) and the Southern Annular Mode (SAM) are relatively clear for future increases of GHGs, with falling pressures over the high latitudes of each hemisphere producing more positive phases of the NAO and SAM (e.g., Arblaster and Meehl 2006; Teng et al. 2006a). However, attributing changes in the NAO or SAM for the latter part of the twentieth century is more difficult. Changes in ozone seem to have made a major contribution to the trend for a more positive SAM late in the twentieth century (e.g., Arblaster and Meehl 2006), but the trends in the NAO are less easy to attribute. For example, analysis of a 62-member ensemble with a global coupled model has shown that the ensemble mean trend in the NAO is nearly zero, but that one member of the ensemble tracks the observed time evolution of the NAO in the last half of the twentieth century almost exactly (Selten et al. 2004). These results suggest that there may be a large stochastic component to low frequency variability associated with the NAO.

A subsequent study has shown that a poleward shift of storm tracks in each hemisphere with increased GHGs contributes to the characteristic pattern of increased SLP in the subtropics and decreased SLP at high latitudes (Yin 2005). These geographic changes in the NAO and SAM in relation to the geographic patterns of sea ice change raise interesting issues of forcing, response, and inherent variability that are beyond the scope of this paper.

What is clear from the present analysis and others (e.g., Meehl et al. 2005b; Teng et al. 2006b) is that, at any point in time, we are committed to a certain amount of climate change and sea level rise in the future. The longer we wait, the greater the future climate change commitment.

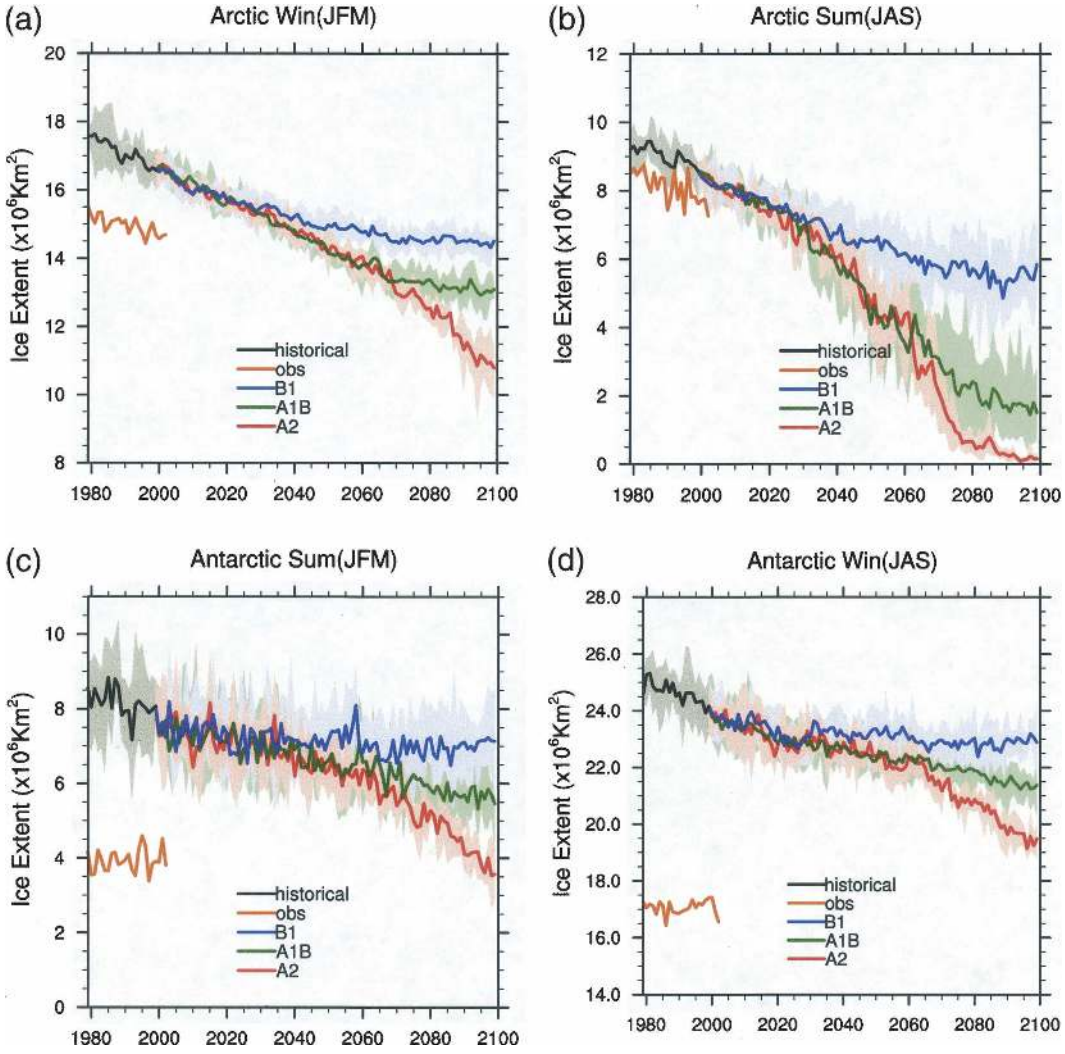

FIG. 12. Seasonal mean sea ice extents ($\times 10^6$ km^2) from observations (Parkinson et al. 1999) and CCSM3 simulations, which include the twentieth-century runs during 1979–2000, and A2 and B1 runs during 2000–99. The shading indicates the spread within the ensemble members for (a) Arctic winter (JFM), (b) Arctic summer (JAS), (c) Antarctic summer (JFM), and (d) Antarctic winter (JAS).

8. Conclusions

The T85 version of the CCSM3 is run for a 1990 control run, and an 1870 control run, which serves as the starting point for eight ensemble member simulations of twentieth-century climate, three SRES scenario experiments for twenty-first-century climate [A2 (five members), A1B, and B1], and three stabilization simulations, one with concentrations held constant at year 2000 values, and two with concentrations held constant at year 2100 values for A1B and B1. The response of the CCSM3 to increasing GHGs depends in part on the equilibrium climate sensitivity of the model, and oceanic heat uptake. Together, these determine the TCR, and the mean value and percent change of the meridional overturning circulation in the Atlantic influence the ocean heat uptake. The global average and geographical plots show we are already committed to significant warming and sea level rise even with no further increases in GHG concentrations. However, any realistic scenario has increases in GHG concentrations, which then further increase the future warming and sea level rise.

These results confirm and quantify earlier studies with simple and global models in that the temperature change commitment is considerably less than the sea level rise commitment by 2100, percentage-wise. That is, temperature increase shows signs of leveling off

100 yr after stabilization, while the sea level continues to rise unabated with proportionately much greater increases compared to temperature, with these committed increases over the twenty-first century roughly an order of magnitude greater for sea level rise than temperature change. The percent increases of committed sea level rise here are roughly 220%, with the changes calculated relative to the respective sea level rise during the twentieth century. Though this is a result that has been acknowledged in other contexts, it is not widely appreciated and is quantified here with multiple CCSM3 simulations. Midlatitude summer drying noted in previous model simulations in a future warmer climate is simulated in the CCSM3, though the relatively small drying does not result in greater soil moisture stress on vegetation in the model.

The distribution of sea ice in each hemisphere is well-simulated by the CCSM3, with, on average, overextensive sea ice but well-simulated sea ice thickness in the Arctic compared to observations. Decreases in sea ice in the future are proportional to the globally averaged warming in the various scenarios. For the high forcing scenario, A2, the Arctic becomes ice-free during summer by the end of the twenty-first century.

Acknowledgments. We acknowledge the efforts of a large group of scientists at NCAR, several DOE labs, and universities across the United States who contributed to the development of the CCSM3 and who participated in formulating the twentieth-century and future climate change simulations through the CCSM working groups on atmosphere, ocean, land surface, polar climate, climate change, climate variability, paleoclimate, biogeochemistry, and software engineering. In particular, we thank Adrian Middleton and Vince Wayland from NCAR, and Michael Wehner at NERSC for their work in either running the model experiments or managing the massive amount of model data. The formidable quantity of supercomputer resources required for this ambitious modeling effort was made available at NCAR through the Initiative Nodes and the Climate System Laboratory, and through the Department of Energy as part of its Advanced Scientific Research (ASCR). ASCR provides computing facilities at NERSC, Los Alamos National Laboratory (LANL) and ORNL Center for Computational Science. Additional simulations with CCSM3 were performed in Japan by the Central Research Institute of the Electric Power Industry (CRIEPI) using the Earth Simulator through the international research consortium of CRIEPI, NCAR, and LANL under the Project for Sustainable Coexistence of Human, Nature, and the Earth of the Japanese Ministry of Education, Culture, Sports, Science, and Technology. We thank Ron Stouffer and an anonymous reviewer for helpful and constructive comments on the manuscript. Portions of this study were supported by the Office of Biological and Environmental Research, U.S. Department of Energy, as part of its Climate Change Prediction Program, and the National Center for Atmospheric Research. This work was also supported in part by the Weather and Climate Impact Assessment Initiative at the National Center for Atmospheric Research.

REFERENCES

Ammann, C. M., G. A. Meehl, W. M. Washington, and C. Zender, 2003: A monthly and latitudinally varying volcanic forcing dataset in simulations of 20th century climate. *Geophys. Res. Lett.,* **30,** 1657, doi:10.1029/2003GL016875.

Arblaster, J. M., and G. A. Meehl, 2006: Contributions of external forcings to Southern Hemisphere Annular Mode trends. *J. Climate,* in press.

Barnett, T. P., D. W. Pierce, K. M. AchutaRao, P. J. Gleckler, B. D. Santer, J. M. Gregory, and W. M. Washington, 2005: Penetration of human-induced warming into the world's oceans. *Science,* doi:10.1126/science.1112418.

Broccoli, A. J., K. W. Dixon, T. L. Delworth, T. R. Knutson, R. J. Stouffer, and F. Zeng, 2003: Twentieth-century temperature and precipitation trends in ensemble climate simulations including natural and anthropogenic forcing. *J. Geophys. Res.,* **108,** 4798, doi:10.1029/2003JD003812.

Bryan, F. O., G. Danabasoglu, N. Nakashiki, Y. Yoshida, D.-H. Kim, J. Tsutsui, and S. C. Doney, 2006: Response of North Atlantic thermohaline circulation and ventilation to increasing carbon dioxide in CCSM3. *J. Climate,* **19,** 2382–2397.

Church, J. A., N. J. White, R. Coleman, K. Lambeck, and J. X. Mitrovica, 2004: Estimates of the regional distribution of sea level rise over the 1950–2000 period. *J. Climate,* **17,** 2609–2625.

Collins, W. D., and Coauthors, 2006a: The Community Climate System Model version 3 (CCSM3). *J. Climate,* **19,** 2122–2143.

——, and Coauthors, 2006b: The formulation and atmospheric simulation of the Community Atmospheric Model: CAM3. *J. Climate,* **19,** 2144–2161.

Cubasch, U., and Coauthors, 2001: Projections of future climate change. *Climate Change 2001: The Scientific Basis: Contribution of Working Group I to the Third Assessment Report of the Intergovernmental Panel on Climate Change,* J. T. Houghton et al., Eds., Cambridge University Press, 525–582.

Dai, A., T. M. L. Wigley, B. A. Boville, J. T. Kiehl, and L. E. Buja, 2001: Climates of the twentieth and twenty-first centuries simulated by the NCAR Climate System Model. *J. Climate,* **14,** 485–519.

——, A. Hu, G. A. Meehl, W. M. Washington, and W. G. Strand, 2005: Atlantic thermohaline circulation in a coupled model: Unforced variations versus forced changes. *J. Climate,* **18,** 3270–3293.

Easterling, D. R., G. A. Meehl, C. Parmesan, S. A. Changnon, T. R. Karl, and L. O. Mearns, 2000: Climate extremes: Observations, modeling, and impacts. *Science,* **289,** 2068–2074.

Folland, C. K., and Coauthors, 2001a: Observed climate variability and change. *Climate Change 2001: The Scientific Basis,* J.

T. Houghton et al., Eds., Cambridge University Press, 99–181.

——, and Coauthors, 2001b: Global temperature change and its uncertainties since 1861. *Geophys. Res. Lett.,* **28,** 2621–2624.

Foukal, P., G. North, and T. Wigley, 2004: A stellar view on solar variations and climate. *Science,* **306,** 68–69.

Gent, P. R., and G. Danabasoglu, 2004: Heat uptake and the thermohaline circulation in the Community Climate System Model, version 2. *J. Climate,* **17,** 4058–4069.

——, F. O. Bryan, G. Danabasoglu, K. Lindsay, D. Tsumune, M. W. Hecht, and S. C. Doney, 2006: Ocean chlorofluorocarbon and heat uptake during the 20th century in the CCSM3. *J. Climate,* **19,** 2366–2381.

Gillett, N. P., H. F. Graf, and T. J. Osborn, 2003: Climate change and the NAO. *The North Atlantic Oscillation*, *Geophysical Monogr.,* No. 134, Amer. Geophys. Union, 193–209.

Gregory, J. M., J. F. B. Mitchell, and A. J. Brady, 1997: Summer drought in northern midlatitudes in a time-dependent CO_2 climate experiment. *J. Climate,* **10,** 662–686.

Hoyt, D. V., and K. H. Schatten, 1993: A discussion of plausible solar irradiance variations, 1700–1992. *J. Geophys. Res.,* **98,** 18 895–18 906.

Hu, A., G. A. Meehl, W. M. Washington, and A. Dai, 2004: Response of the Atlantic thermohaline circulation to increased atmospheric CO_2 in a coupled model. *J. Climate,* **17,** 4267–4279.

Kiehl, J. T., and P. R. Gent, 2004: The Community Climate System Model, version 2. *J. Climate,* **17,** 3666–3682.

——, T. L. Schneider, R. W. Portman and S. Solomon, 1999: Climate forcing due to tropospheric and stratospheric ozone. *J. Geophys. Res.,* **104,** 31 239–31 254.

——, C. A. Shields, J. J. Hack, and W. Collins, 2006: The Climate Sensitivity of the Community Climate System Model version 3 (CCSM3). *J. Climate,* **19,** 2584–2596.

Lamarque, J.-F., P. Hess, L. Emmons, L. Buja, W. Washington, and C. Granier, 2005: Tropospheric ozone evolution between 1890 and 1990. *J. Geophys. Res.,* **110,** D08304, doi:10.1029/2004JD005537.

Lawrence, D. M., and A. G. Slater, 2005: A projection of severe near-surface permafrost degradation during the 21st century. *Geophys. Res. Lett.,* **32,** L24401, doi:10.1029/2005GL025080.

Lean, J., J. Beer, and R. Bradley, 1995: Reconstruction of solar irradiance since 1610: Implications for climate change. *Geophys. Res. Lett.,* **22,** 655–658.

——, Y.-M. Wang, and N. R. Sheeley Jr., 2002: The effect of increasing solar activity on the sun's total open magnetic flux during multiple cycles: Implications for solar forcing of climate. *Geophys. Res. Lett.,* **29,** 2002, doi:10.1029/2002GL015880.

Levitus, S., J. Antonov, and T. Boyer, 2005: Warming of the world ocean, 1953–2003. *Geophys. Res. Lett.,* **32,** L02604, doi:10.1029/2004GL021592.

Manabe, S., and R. J. Stouffer, 1999: The role of thermohaline circulation in climate. *Tellus,* **51A-B,** 91–109.

Meehl, G. A., and W. M. Washington, 1996: El Nino-like climate change in a model with increased atmospheric CO_2 concentrations. *Nature,* **382,** 56–60.

——, W. D. Collins, B. Boville, J. T. Kiehl, T. M. L. Wigley, and J. M. Arblaster, 2000: Response of the NCAR Climate System Model to increased CO_2 and the role of physical processes. *J. Climate,* **13,** 1879–1898.

——, W. M. Washington, C. Ammann, J. M. Arblaster, T. M. L. Wigley, and C. Tebaldi, 2004a: Combinations of natural and anthropogenic forcings and 20th century climate. *J. Climate,* **17,** 3721–3727.

——, C. Covey, M. Latif, B. McAvaney, and R. J. Stouffer, 2004b: Soliciting participation in the climate model analyses leading to the IPCC Fourth Assessment Report. *Eos, Trans. Amer. Geophys. Union,* **29,** 274.

——, W. M. Washington, J. M. Arblaster, and A. Hu, 2004c: Factors affecting climate sensitivity in global coupled models. *J. Climate,* **17,** 1584–1596.

——, C. Covey, B. McAvaney, M. Latif, and R. J. Stouffer, 2005a: Overview of the Coupled Model Intercomparison Project. *Bull. Amer. Meteor. Soc.,* **86,** 89–93.

——, W. M. Washington, W. D. Collins, J. M. Arblaster, A. Hu, L. E. Buja, W. G. Strand, and H. Teng, 2005b: How much more global warming and sea level rise? *Science,* **307,** 1769–1772.

Miller, L., and B. C. Douglas, 2004: Mass and volume contributions to twentieth-century global sea level rise. *Nature,* **428,** 406–409.

Mitchell, J. F. B., T. C. Johns, W. J. Ingram, and J. A. Lowe, 2000: The effect of stabilising atmospheric carbon dioxide concentrations on global and regional climate change. *Geophys. Res. Lett.,* **27,** 2977–2980.

Parkinson, C. L., D. J. Cavalieri, P. Gloersen, H. J. Zwally, and J. C. Comiso, 1999: Arctic sea ice extents, areas, and trends, 1978–1996. *J. Geophys. Res.,* **104,** 20 837–20 856.

Ramanathan, V., 1988: The greenhouse theory of climate change: A test by an inadvertent global experiment. *Science,* **240,** 293–299.

Raper, S. C. B., J. M. Gregory, and R. J. Stouffer, 2002: The role of climate sensitivity and ocean heat uptake on AOGCM transient temperature response. *J. Climate,* **15,** 124–130.

Rayner, N. A., D. E. Parker, E. B. Horton, C. K. Folland, L. V. Alexander, D. P. Rowell, E. C. Kent, and A. Kaplan, 2003: Global analyses of sea surface temperature, sea ice, and night marine air temperature since the late nineteenth century. *J. Geophys. Res.,* **108,** 4407, doi:10.1029/2002JD002670.

Selten, F. M., G. W. Branstator, H. A. Dijkstra, and M. Kliphuis, 2004: Tropical origins for recent and future Northern Hemisphere climate change. *Geophys. Res. Lett.,* **31,** L21205, doi:10.1029/2004GL020739.

Seneviratne, S. I., J. S. Pal, E. A. B. Eltahir, and C. Schär, 2002: Summer dryness in a warmer climate: A process study with a regional climate model. *Climate Dyn.,* **20,** 69–85.

Smith, S. J., H. Pitcher, and T. M. L. Wigley, 2001: Global and regional anthropogenic sulfur dioxide emissions. *Global Planet. Change,* **29,** 99–119.

——, R. Andres, E. Conception, and J. Lurz, 2004: Sulfur dioxide emissions: 1850–2000. Tech. Rep. PNNL-14537, JGCRI, 16 pp.

——, H. Pitcher, and T. M. L. Wigley, 2005: Future sulfur dioxide emissions. *Climatic Change,* **73,** 267–318.

Stouffer, R. J., 2004: Time scales of climate response. *J. Climate,* **17,** 209–217.

——, and S. Manabe, 1999: Response of a coupled ocean–atmosphere model to increasing atmospheric carbon dioxide: Sensitivity to the rate of increase. *J. Climate,* **12,** 2224–2237.

——, and Coauthors, 2006: Investigating the causes of the response of the thermohaline circulation to past and future climate changes. *J. Climate,* **19,** 1365–1387.

Stott, P. A., S. F. B. Tett, G. S. Jones, M.-R. Allen, J. E. B. Mitchell, and G. J. Jenkins, 2000: External control of 20th

century temperature by natural and anthropogenic forcings. *Science ,* **290,** 2133–2137.

Teng, H., W. M. Washington, G. A. Meehl, L. A. Buja, and G. W. Strand, 2006a: 21st century arctic climate change in the CCSM3 IPCC scenario simulations. *Climate Dyn.,* doi;10.1007/S00382-005-0099-z.

——, L. E. Buja, and G. A. Meehl, 2006b: 20th-century climate change commitment from 12 general circulation models. *Geophys. Res. Lett.,* in press.

Wetherald, R. T., and S. Manabe, 1995: The mechanisms of summer dryness induced by greenhouse warming. *J. Climate,* **8,** 3096–3108.

——, and ——, 2002: Simulation of hydrologic changes associated with global warming. *J. Geophys. Res.,* **107,** 4379, doi:10.1029/2001JD001195.

——, R. J. Stouffer, and K. W. Dixon, 2001: Committed warming and its implications for climate change. *Geophys. Res. Lett.,* **28,** 1535–1538.

Wigley, T. M. L., 2005: The climate change commitment. *Science,* **307,** 1766–1769.

——, and S. Raper, 2003: Future changes in global-mean temperature and sea level. *Climate and Sea Level Change: Observations, Projections and Implications* R. A. Warrick, E. M. Barrow, and T. M. L. Wigley, Eds., Cambridge University Press, 111–133.

——, S. J. Smith, and M. J. Prather, 2002: Radiative forcing due to reactive gas emissions. *J. Climate,* **15,** 2690–2696.

Yin, J. H., 2005: A consistent poleward shift of the storm tracks in simulations of 21st century climate. *Geophys. Res. Lett.,* **32,** L18701, doi:10.1029/2005GL023684.

Yoshida, Y., K. Maruyama, J. Tsutsui, N. Nakashiki, F. O. Bryan, M. Blackmon, B. A. Boville, and R. D. Smith, 2005: Multicentury ensemble global warming projections using the Community Climate System Model (CCSM3) *J. Earth Sim.,* **3,** 2–10.